For longer processes and fluorescent objects comparable to or bigger than the tip, quenching can be further avoided by conducting measurements under liquid, where the frictional forces associated with the shear-force feedback mechanism allow for larger tip-sample separations (9). The fact that time-resolved fluorescence measurements on single chromophores can be performed in a nonpurtabative manner opens the way toward the study of chemical reactions on a single-molecule basis. Detailed studies of dynamical processes—such as photoinduced electron transfer, proton transfer, isomerization, or protein conformational changes—in specific local environments with known molecular orientations are now experimentally feasible.

REFERENCES AND NOTES

1. W. E. Moerner and L. Kador, *Phys. Rev. Lett.* **62**, 2535 (1989).
2. M. Oritt and J. Bernard, *ibid.* **65**, 2716 (1990).
3. E. B. Shera, N. K. Seitzinger, L. M. Davis, R. A. Keller, S. A. Soper, *Chem. Phys. Lett.* **174**, 553 (1990).
4. M. D. Barnes, K. C. Nig, W. B. Whitten, J. M. Ramsey, *Anal. Chem.* **65**, 2360 (1993).
5. A. Castro and B. Shera, in *Laser Applications to Chemical Analysis,* vol. 5 of *Technical Digest Series* (Optical Society of America, Washington, DC, 1994), p. 210.
6. E. Betzig and R. J. Chichester, *Science* **262**, 1422 (1993).
7. W. P. Ambrose, P. M. Goodwin, J. C. Martin, R. A. Keller, *Phys. Rev. Lett.* **72**, 132 (1994).
8. J. K. Trautman, J. J. Macklin, L. E. Brus, E. Betzig, *Nature* **369**, 40 (1994).
9. X. S. Xie, E. V. Allen, G. R. Holtom, R. C. Dunn, L. Mets, in *Proc. SPIE* **2137**, 264 (1994).
10. E. Betzig and J. K. Trautman, *Science* **257**, 189 (1992); D. W. Pohl, in *Advances in Optical and Electron Microscopy*, T. Mulvey and C. J. R. Sheppard, Eds. (Academic Press, New York, 1991), vol. 12, pp. 243–312.
11. R. C. Dunn, G. R. Holtom, L. Mets, X. S. Xie, *J. Phys. Chem.* **98**, 3094 (1994).
12. W. P. Ambrose, P. M. Goodwin, J. C. Martin, R. A. Keller, *Proc. SPIE* **2125**, 2 (1994).
13. E. Betzig, J. K. Trautman, T. D. Harris, J. S. Weiner, R. L. Kostelak, *Science* **251**, 1468 (1991).
14. U. Durig, D. W. Pohl, F. Rohner, *J. Appl. Phys.* **59**, 3318 (1986).
15. E. Betzig, P. L. Finn, J. S. Weiner, *Appl. Phys. Lett.* **60**, 2484 (1992).
16. R. Toledo-Crow, P. C. Yang, Y. Chen, M. Vaez-Iravani, *ibid.*, p. 2957.
17. R. C. Dunn, E. V. Allen, S. A. Joyce, G. A. Anderson, X. S. Xie, *Ultramicroscopy*, in press.
18. The tip feedback and *xy* scanner are interfaced with a Nanoscope III controller (Digital Instruments). The near-field assembly and sample stage are built onto an inverted fluorescence microscope (Nikon Diaphot). The optics train is as follows: linearly polarized 594-nm HeNe laser (Particle Measuring Sytems, bandwidth <1 GHz); optical shutter; acousto-optic intensity stabilizer (LiCONix), holographic bandpass prism (Kaiser Optical Systems); variable neutral density filter (Reynard); λ/2 and λ/4 plates (Newport); fiber coupler (Newport, ×20 objective lens); 2 m of single mode fiber (Corning Flexcore 633) with the near-field probe at the end; transparent sample; oil immersion objective lens (Nikon, ×100, numerical aperture 1.3); holographic beam splitter and holographic notch plus filter for 594 nm (Kaiser Optical Systems); optics inside the inverted fluorescence microscope directing the emission to the output port; dielectric filter (Corion LS-950.S.1166F, for rejection of scattered 1.15-μm light from a HeNe laser used for shear-force feedback); 3-cm focal lens; and an avalanche photodiode detector [EG&G Canada, #SPCM-200 modified for fast time response (*19*)]. The sample was prepared by dispersing a dilute methanol solution of sulforhodamine 101 (Exciton) (2×10^{-9} M) on a borosilicate glass cover slip (Becton Dickinson, no. 3305). All experiments were performed on dry sample at room temperature.
19. L. Li and L. M. Davis, *Rev. Sci. Instrum.* **64**, 1524 (1993).
20. H. A. Bethe, *Phys. Rev.* **66**, 163 (1944).
21. C. J. Bouwkamp, *Philips Res. Rep.* **5**, 321 (1950); *ibid.*, p. 401.
22. M. Lieberherr, C. Fattinger, W. Lukosz, *Surf. Sci.* **189**, 954 (1987).
23. W. P. Ambrose and W. E. Moerner, *Nature* **349**, 225 (1991); W. E. Moerner and T. Basche, *Angew. Chem.* **32**, 457 (1993); P. T. Tchenio, A. B. Myers, W. E. Moerner, *J. Lumin.* **56**, 1 (1993).
24. M. Pirotta *et al.*, *Chem. Phys. Lett.* **208**, 379 (1993).
25. S. A. Soper, L. M. Davis, E. B. Shera, *J. Opt. Soc. Am. B.* **9**, 1761 (1992).
26. J. A. Lakowicz, H. Szmacinski, K. Nowaczyk, M. L. Johnson, *Proc. Natl. Acad. Sci. U.S.A.* **89**, 1271 (1992).
27. X. F. Wang, A. Periasamy, B. Herman, D. M. Coleman, *Crit. Rev. Anal. Chem.* **23**, 369 (1992).
28. R. R. Chance, A. Prock, R. Silbey, *Adv. Chem. Phys.* **37**, 1 (1978).
29. K. H. Drexahage, in *Progress in Optics XII*, E. Wolf, Ed., (North-Holland, New York, 1974), p. 165.
30. P. Avouris and B. N. J. Persson, *J. Phys. Chem.* **88**, 837 (1984); B. N. J. Persson and N. D. Lang, *Phys. Rev. B* **26**, 5409 (1982); B. N. J. Persson and M. Persson, *Surf. Sci.* **97**, 609 (1980); B. N. J. Persson, *J. Phys. C* **11**, 4251 (1978).
31. G. Cnossen, K. E. Drabe, D. A. Wiersma, *J. Chem. Phys.* **98**, 5276 (1993).

32. We thank G. Anderson for designing the multidimensional histogram electronics, E. Vey Allen for his assistance in the development of the microscope, S. D. Colson for stimulating discussions, G. Holtom for assistance with time-correlated photon counting, and Digital Instruments for their support. This work was supported by the Chemical Sciences Division of the Office of Basic Energy Sciences and in part by Laboratory Technology Transfer Program within the Office of Energy Research of the U.S. Department of Energy (DOE). Pacific Northwest Laboratory is operated for DOE by Battelle Memorial Institute under contract DE-AC06-76RLO 1830.

8 April 1994; accepted 17 May 1994

Alterations of Single Molecule Fluorescence Lifetimes in Near-Field Optical Microscopy

W. Patrick Ambrose,* Peter M. Goodwin, John C. Martin, Richard A. Keller

Fluorescence lifetimes of single Rhodamine 6G molecules on silica surfaces were measured with pulsed laser excitation, time-correlated single photon counting, and near-field scanning optical microscopy (NSOM). The fluorescence lifetime varies with the position of a molecule relative to a near-field probe. Qualitative features of lifetime decreases are consistent with molecular excited state quenching effects near metal surfaces. The technique of NSOM provides a means of altering the environment of a single fluorescent molecule and its decay kinetics in a repeatable fashion.

Experiments on single molecules reveal details of molecular environments that are indiscernible in bulk measurements. Optical single molecule detection has been reported in liquids (*1–6*), in solids (*7–11*), and on surfaces (*12–16*), where single molecules are used as probes of individual local environments and as indicators of unimolecular events. The technique used to detect single molecules on surfaces under ambient conditions, NSOM, is a scanned probe microscopy that uses a subwavelength optical aperture to illuminate a subdiffraction limited area on a surface (*17*). In NSOM, small areas are illuminated with high irradiance and low power. Single molecule sensitivity is attained because the background scattered light, which is a fixed fraction of the excitation power, is accordingly low. Single fluorescent molecules were used to probe the optical electric field distribution around a near-field aperture with a diameter of ~50 nm (*12*). Photobleaching of individual molecules was observed directly as an abrupt cessation of fluorescence under irradiation from a near-field source (*13*).

We demonstrate the use of pulsed excitation and time-correlated single photon counting (TCSPC) to resolve temporally the fluorescence from individual Rhodamine 6G (R6G) molecules on silica located <10 nm from an NSOM probe. In TCSPC, the elapsed time between an excitation pulse and a detected photon is measured. A histogram of the elapsed times provides a fluorescence decay curve, from which the fluorescence lifetime (τ) is extracted. As a single R6G molecule is moved near an NSOM probe, τ varies repeatably with position under the probe. Qualitative features of some alterations in τ are consistent with

W. P. Ambrose, P. M. Goodwin, R. A. Keller, Chemical Science and Technology Division, Los Alamos National Laboratory, Los Alamos, NM 87545, USA.
J. C. Martin, Life Sciences Division, Los Alamos National Laboratory, Los Alamos, NM 87545, USA.

*To whom correspondence should be addressed.

molecular excited state quenching effects near metal surfaces (*18*).

Combining TCSPC with time-gated detection decreases the background noise in our NSOM images by a factor of 3 and increases the typical signal-to-noise ratio (S/N) by a factor of 1.4. The S/N is improved because prompt background scatter and fluorescence photons are separated temporally and much of the background and its associated noise are not counted (*19*).

Sample preparation, NSOM, and TCSPC, previously described (*1–3, 13*), are summarized below. Samples were fused silica disks spin-coated with either 3×10^{-9} M or 10^{-6} M R6G-methanol solutions. The average molecular spacings were ~1000 or 70 nm (*20, 21*) (referred to, respectively, below as low- or high-coverage surfaces). We constructed NSOM probes by tapering one end of single mode optical fibers (~30 cm long) and coating them with an opaque aluminum film (~150 nm thick), leaving a small aperture at the tip (*13, 22*). Scanning electron microscope images show that the faces of coated probes are nearly flat and 500 to 600 nm in diameter. Hence, a probe face consists of a glass aperture 200 to 300 nm in diameter within an aluminum annulus 150 nm wide. For NSOM imaging, a sample surface was raster-scanned under a probe and shear force feedback was used to control the tip-surface height to <10 nm (*13, 23*). Laser light coupled into the single mode fiber emerged from the aperture and illuminated the surface. The laser was a mode-locked Ar^+ laser operated at a wavelength of 514.5 nm with a pulse repetition rate of 82 MHz and a pulse width of ~150 ps. Fluorescence emitted from molecules on the silica surface was collected with a ×100, 1.3 numerical aperture, oil immersion microscope objective and was detected with a photon-counting, silicon avalanche photodiode (APD) (*6, 14, 24*). We counted the APD pulses using TCSPC techniques (*1–3*).

An example of a fluorescence image obtained on a low-coverage surface is shown in Fig. 1A. The two-lobed feature, a, is a stable fluorescence image formed by a single R6G molecule (*25*). By stable, we mean that the fluorescence intensities were reproducible over many minutes. About 100 spatially well-separated, two-lobed images were observed in 8 μm by 8 μm images (*14*). The lobe orientations are aligned with and follow the far-field polarization (*14*); the two lobes belong to the near-field image of a single molecule. Some molecules show intensity variations on time scales less than a minute (*13*). For example, feature b has a dark line through the lower lobe and feature c has a noisy appearance. A shear force image obtained concurrently with Fig. 1 shows no feedback instability other than 2-nm peak-to-peak height noise throughout the image. The fluctuations in features b and c are attributed to small motions of the molecules that change their optical dipole orientations and thus their absorption and emission rates (*13*). There is a terminated feature at d, which is seen as an abrupt loss of signal to the background during a line scan (Fig. 1B). In similar experiments, terminated features were missing in subsequent images. We interpret these as molecules that photobleach during imaging (*13*).

The following evidence supports the idea that these fluorescent features arise from single R6G molecules. (i) A control experiment in which one probe and three samples (one with R6G, the next without, and a third with R6G) were used indicates that the fluorescence arises from R6G. (ii) Many features of the same lateral extent are observed with a number density within an order of magnitude of expected values. (iii) The individual R6G features have polarization-dependent absorption characteristics (*14*). (iv) With constant excitation, individual R6G features disappear abruptly (photobleach) and are missing in subsequent fluorescence images (*13*) (loose clusters of molecules would show many photobleaching steps). (v) The measured photobleaching efficiencies (*13*) (10^{-7} to 10^{-6}) are within the previously measured range (*26*) (10^{-7} to 10^{-5}). (vi) The fluorescence decays are fitted well by single exponentials (see below). Taken together, this evidence is consistent with the detection of single R6G molecules and is inconsistent with the

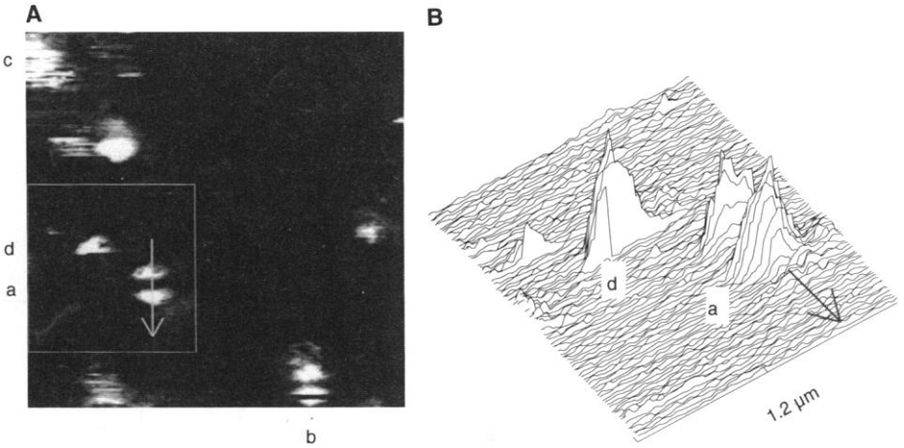

Fig. 1. (**A**) Fluorescence NSOM image of single R6G molecules on silica. The image size is 2.6 μm by 2.7 μm (200 by 200 pixels). (**B**) Surface plot of the box in (A), scanned from left to right, starting at the top. The power in the far field was 34 nW, and the polarization was vertical. The peaks in the surface plot are ~250 photocounts per 20 ms high. The single molecule features are ~200 to 350 nm wide, indicating that the tip aperture is ~300 nm. The arrows show the path across the two-lobed image (feature a) of a single R6G molecule used for τ measurements (Fig. 4, molecule a).

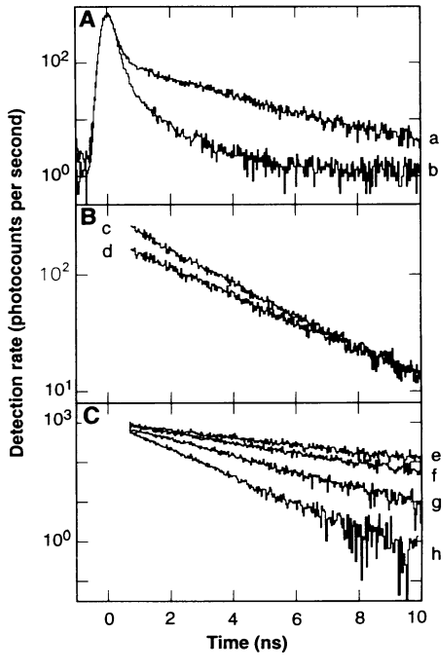

Fig. 2. Time-correlated single photon counting-rate histograms. (**A**) Plots obtained from (trace a) a single R6G molecule on silica and (trace b) a bare silica substrate (background) <10 nm under an NSOM probe. (**B**) Decays obtained for a higher coverage surface with the tip at a distance of (trace c) <10 nm and (trace d) 1.1 μm above the surface. (**C**) Traces obtained at lateral positions of maximum fluorescence intensity (±10 nm) over different single R6G molecules. The extracted τ values are (trace e) 4.6, (trace f) 3.4, (trace g) 2.1, and (trace h) 1.3 ns. The rates in (C) are normalized to 10^3 per second at zero time for slope comparisons. Background traces were subtracted in (B) and (C). Far-field powers: (A) 33 nW, (B) 1.8 nW, and (C) ~20 nW. Maximum counts per bin for each trace: (a) 3011, (b) 4804, (c) 5215, (d) 6605, (e) 2667, (f) 8588, (g) 10,407, and (h) 19,474. The bin width is 30.8 ps.

detection of closely or loosely associated aggregates of R6G molecules.

Pulsed excitation and time-gated detection lead to improved S/N (Fig. 2). The peaks in ungated histograms (at zero time) for a typical R6G molecule (trace a) and the bare silica substrate (trace b) at a distance <10 nm from an NSOM probe are primarily prompt Raman scattered light generated in the 30-cm optical fiber of the probe. After the peak, trace b shows a weak tail of constant background. The tail in trace a above the background is fluorescence from a single R6G molecule.

For rejection of the prompt background in emission rate measurements, a time window is opened from 0.7 to 10 ns after the peak, and only photons satisfying this gate are counted. Time gating decreases the integrated background by an order of magnitude and the noise in the background by a factor of 3 [the entire background is 390 photocounts per second per nanowatt (count s^{-1} nW^{-1}) and the gated background in the tail is 42 count s^{-1} nW^{-1}]. The ungated single molecule signal (background subtracted) is 225 count s^{-1} nW^{-1}, and the gated signal is 200 count s^{-1} nW^{-1} in Fig. 2, trace a (for other molecules, this value ranges up to ~600). From Fig. 2A, the integrated S/N without gating is $225/(225 + 390)^{1/2} = 9(Hz/nW)^{1/2}$, and the gated S/N is $200/(200 + 42)^{1/2} = 13$ $(Hz/nW)^{1/2}$. With 30-nW excitation power measured in the far field and a 50-Hz counting bandwidth, the typical gated S/N is ~10.

The goal of this work was to measure the perturbation of τ caused by the presence of an NSOM probe. We performed experiments on populations of molecules to obtain the mean, unperturbed lifetime $\langle\tau\rangle$ and limits on the width in the distribution of τ. Five unperturbed fluorescence decay curves were measured for tips positioned 1.0 to 1.1 μm above higher coverage surfaces (~10^3 to 10^4 molecules illuminated) (Fig. 2, trace d). The decay curves were fitted well by a single exponential with $\langle\tau\rangle = 3.65 \pm 0.04$ ns, which is in good agreement with the value 3.5 ± 0.1 ns obtained previously (*26*). Statistical noise and instrument nonlinearity place an upper limit on a possible Gaussian standard deviation of τ values, σ, of $\sigma/\langle\tau\rangle = 0.2$, which is consistent with theoretical limits on σ for single decay data with noise (*27*). A high-coverage surface was then moved into the near field (<10 nm from the probe face) (Fig. 2, trace c). Approximately 25 molecules were distributed in the near field, and the decay is more nonlinear (on this semilogarithmic plot) than the bulk decay. The far-field, bulk decay curves could be consistent with an inhomogeneous distribution of lifetimes with width <20% of the mean. This width increases in the near field.

Using a low-coverage surface, we positioned single R6G molecules within the near field such that the fluorescence intensity was maximized, and data were collected until each molecule photobleached (yielding from 10^3 to 10^5 photocounts). Depending on the orientation of each molecule, maximum fluorescence corresponds to different positions under the tip (*12*). Examples of fluorescence decay curves from individual R6G molecules are shown in Fig. 2C. Measurements on 17 different molecules were made, and each was fitted well by a single exponential. A histogram of these τ values is shown in Fig. 3. Because these molecules were at different positions under the tip, position-dependent measurements were made on individual molecules.

Single molecules were moved laterally across the face of the NSOM tip, and emission rate and τ were measured at fixed sample displacements (Fig. 4). These experiments were attempted on many molecules, and eight molecules did not photobleach during the measurements (each data set contains ~10^5 photocounts). The data were obtained at two far-field power levels differing by a factor of 8 to 9. The emission rates (Fig. 4A) scale approximately with the power, indicating that the higher irradiance is below the saturation value. Fluorescence decay data were obtained concurrently at each position for both power levels, and the single exponential lifetimes were calculated (Fig. 4B). Near the metal coating at the edges of the aperture (~±150 nm), τ is short, and as a molecule is moved inward away from the metal coating, τ increases. The τ values do not depend on power (the triangles and circles overlap in Fig. 4B) and therefore are not a function of the tip temperature or near-field irradiances used. The range of τ values obtained by moving eight different molecules under the probe face (Fig. 3) shows that the fluorescence lifetime of an R6G molecule is altered as an NSOM probe moves over the molecule.

Metal surfaces near radiating dipoles are known to influence fluorescence lifetimes (*18*). Two distinct physical phenomena were identified (*18*): fluorescence quenching and spontaneous emission modification. (i) At short distances (<50 nm), nonradiative energy transfer from a molecule to electrons in the metal dominates the excited state decay rate, and τ approaches zero with decreasing distance. (ii) When an emitting molecule is within a distance of about one emission wavelength from the metal (~550 nm), the emission rate is influenced by the radiation reflected from the surface. Spontaneous emission is suppressed or enhanced depending on the phase and strength of the reflected field,

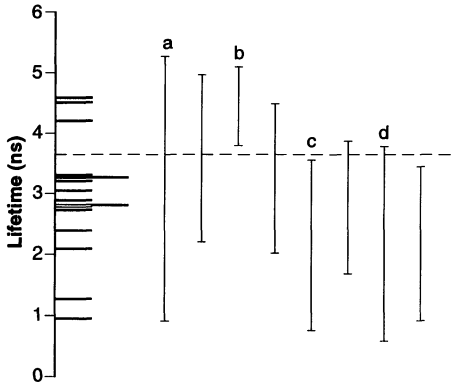

Fig. 3. Summary of single molecule lifetime data. On the left is a histogram of single exponential decay times obtained at the positions of maximum fluorescence over 17 different R6G molecules. The dashed line is the measured bulk lifetime, $\langle\tau\rangle = 3.65$ ns. The eight spans show the range of lifetime values resulting from scans of eight different molecules under an NSOM probe. The four labeled spans correspond to measurements for molecules a through d in Fig. 4B.

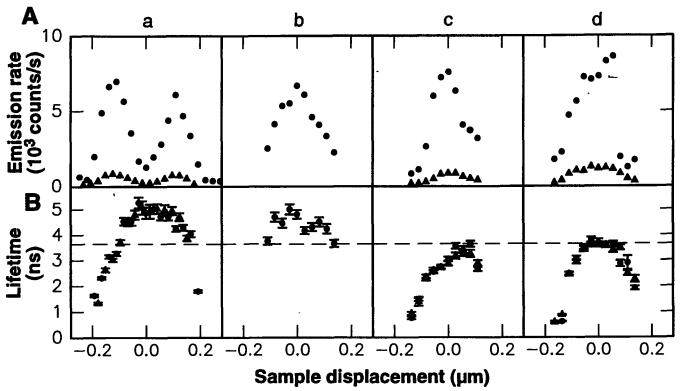

Fig. 4. (**A**) Emission rate and (**B**) fluorescence lifetime versus lateral displacement for four different R6G molecules (a through d). Molecule a corresponds to feature a in Fig. 1. We relocated single molecules identified in image scans using a search routine while monitoring the fluorescence signal. The tip was maintained <10 nm from the surface throughout these measurements (the height noise was ~2 nm peak to peak). At each position separated by ~27 nm, 7938 photocounts were obtained. Error bars on the τ data are confidence limits on single exponential fits. Far-field power levels: molecule a, (●) 22 and (▲) 2.5 nW; molecule b, (●) 38 nW; molecule c, (●) 31 and (▲) 3.8 nW; and molecule d, (●) 42 and (▲) 4.9 nW.

and in this region, τ oscillates with distance about the value measured at large separation [this effect can be described either as classical modifications or cavity quantum electrodynamic effects in a "bad cavity" as defined in (*28*)].

Some of the maximum values near the middle are well above the far-field bulk $\langle\tau\rangle$ (compare ranges in Fig. 3 to the dashed line). Two factors may contribute to values larger than the bulk lifetime: (i) There could be an inhomogeneous distribution of unperturbed τ values, or (ii) spontaneous emission suppression may affect τ near the center of the probe. An independent means of measuring unperturbed single molecule lifetimes is needed to establish the level of perturbation in the center of the probe. Near the metal edges of the aperture, τ is decreased by at least a factor of 3; fluorescence certainly is quenched near the metal edges.

Our results highlight an important aspect of single molecule experiments; namely, a single molecule can be used as a point probe that displays dramatic fluorescence lifetime variations near an NSOM probe, whereas ensemble measurements only provide spatially averaged information. Because the lifetime variations are repeatable, NSOM provides a means of altering the environment of a single molecule and its decay kinetics. Single molecule NSOM experiments will provide important tests for near-field theories that incorporate the physical effects of radiators near metallic structures. In addition, single molecules will be useful as calibration probes for individual NSOM tips.

Note added in proof: Single molecule detection by conventional optical microscopy was recently reported (*29*). This method could be used as an independent technique to explore unperturbed inhomogeneous lifetime distributions.

REFERENCES AND NOTES

1. E. B. Shera, N. K. Seitzinger, L. M. Davis, R. A. Keller, S. A. Soper, *Chem. Phys. Lett.* **174**, 553 (1990).
2. C. W. Wilkerson, P. M. Goodwin, W. P. Ambrose, J. C. Martin, R. A. Keller, *Appl. Phys. Lett.* **62**, 2030 (1993).
3. P. M. Goodwin, C. W. Wilkerson, W. P. Ambrose, R. A. Keller, *Proc. SPIE* **1895**, 79 (1993).
4. M. D. Barnes, K. C. Ng, W. B. Whitten, J. M. Ramsey, *Anal. Chem.* **65**, 2360 (1993).
5. R. Rigler, J. Widengren, Ü. Mets, in *Fluorescence Spectroscopy: New Methods and Applications*, O. S. Wolfbeis, Ed. (Springer-Verlag, Berlin, 1993), p. 13.
6. S. A. Soper, Q. L. Mattingly, P. Vegnuta, *Anal. Chem.* **65**, 740 (1993).
7. W. E. Moerner and L. Kador, *Phys. Rev. Lett.* **62**, 2535 (1989).
8. M. Orrit and J. Bernard, *ibid.* **65**, 2716 (1990).
9. W. P. Ambrose and W. E. Moerner, *Nature* **349**, 225 (1991).
10. W. E. Moerner and T. Basché, *Angew. Chem. Int. Ed. Engl.* **32**, 457 (1993).
11. M. Pirotta *et al.*, *Chem. Phys. Lett.* **208**, 379 (1993).
12. E. Betzig and R. J. Chichester, *Science* **262**, 1422 (1993).
13. W. P. Ambrose, P. M. Goodwin, J. C. Martin, R. A. Keller, *Phys. Rev. Lett.* **72**, 160 (1994).
14. ———, *Proc. SPIE* **2125**, 2 (1994).
15. R. C. Dunn, E. V. Allen, S. A. Joyce, G. A. Anderson, X. S. Xie, *Ultramicroscopy*, in press.
16. J. K. Trautman, J. J. Macklin, L. E. Brus, E. Betzig, *Nature* **369**, 40 (1994).
17. U. Dürig, D. W. Pohl, F. Rohner, *J. Appl. Phys.* **59**, 3318 (1986).
18. K. H. Drexhage, *Prog. Opt.* **12**, 163 (1974).
19. N. K. Seitzinger, K. D. Hughes, F. E. Lytle, *Anal. Chem.* **61**, 2611 (1989).
20. D. C. Nguyen, R. E. Muenchausen, R. A. Keller, N. S. Nogar, *Opt. Commun.* **60**, 111 (1986).
21. M. Lieberherr, C. Fattinger, W. Lukosz, *Surf. Sci.* **189**, 954 (1987).
22. E. Betzig, J. K. Trautman, T. D. Harris, J. S. Weiner, R. L. Kostelak, *Science* **251**, 1468 (1991).
23. E. Betzig and J. K. Trautman, *ibid.* **257**, 189 (1992).
24. L. Q. Li and L. M. Davis, *Rev. Sci. Instrum.* **64**, 1524 (1993).
25. The reason for the multiply lobed images was described in (*12*): An optical dipole is excited by the component of the field along the dipole axis. The field bows out from the aperture and is normal to the aperture edges. A single optical dipole oriented perpendicular to the aperture is excited most strongly by the edge fields, and lobes form as the point-like molecule images one component of the near field.
26. A. L. Huston and C. T. Reimann, *Chem. Phys.* **149**, 401 (1991).
27. J. N. Demas and B. A. DeGraff, *Sensors Actuators B* **11**, 35 (1993).
28. T. W. Mossberg and M. Lewenstein, in *Cavity Quantum Electrodynamics*, P. R. Berman, Ed. (Academic Press, Boston, MA, 1994), p. 173.
29. M. Ishikawa, K. Hirano, T. Hayakawa, S. Hosoi, S. Brenner, *Jpn. J. Appl. Phys.* **33**, 1571 (1994).

9 March 1994; accepted 31 May 1994

Fine Structure of the Landers Fault Zone: Segmentation and the Rupture Process

Yong-Gang Li,* John E. Vidale, Keiiti Aki, Chris J. Marone, William H. K. Lee

Observations and modeling of 3- to 6-hertz seismic shear waves trapped within the fault zone of the 1992 Landers earthquake series allow the fine structure and continuity of the zone to be evaluated. The fault, to a depth of at least 12 kilometers, is marked by a zone 100 to 200 meters wide where shear velocity is reduced by 30 to 50 percent. This zone forms a seismic waveguide that extends along the southern 30 kilometers of the Landers rupture surface and ends at the fault bend about 18 kilometers north of the main shock epicenter. Another fault plane waveguide, disconnected from the first, exists along the northern rupture surface. These observations, in conjunction with surface slip, detailed seismicity patterns, and the progression of rupture along the fault, suggest that several simple rupture planes were involved in the Landers earthquake and that the inferred rupture front hesitated or slowed at the location where the rupture jumped from one to the next plane. Reduction in rupture velocity can tentatively be attributed to fault plane complexity, and variations in moment release can be attributed to variations in available energy.

The major crustal faults that accommodate tectonic motion are complex sets of slip planes, which are probably influenced by the presence of fault gouge and fluid, and exhibit deformation that ranges from steady to stick-slip (*1*). The part of the fault that slips at depth in an earthquake is quite narrow, so it is difficult to delineate the features that make faults segment into distinct earthquakes. Recently, short-wavelength seismic waves that travel mainly within the fault zone have been detected (*2*). Because the fault zone is characterized by slower velocities than the surrounding intact rock, probably as a result of intense brecciation and possibly high fluid pressure, it forms a waveguide. When an earthquake occurs in the fault zone, some seismic energy is trapped in the waveguide and propagates as normal modes that are formed by the constructive interference of the multiple reflections at boundaries between the low-velocity fault zone and the high-velocity surrounding rock. Such waves are similar to surface or channel waves.

In this report, we illustrate fault zone–guided waves from aftershocks of the Landers earthquakes (*3*, *4*). On the basis of the observation and modeling of the guided waves, we document the fine velocity structure in the heart of the fault zone that ruptured in the 28 June 1992 magnitude M7.4 Landers earthquake.

In the months after the main shock, linear seismic arrays crossing the fault trace were installed at nine locations along the rupture plane for the purpose of detecting fault-guided waves (*3*, *4*). The array at recording site 8 had 22 three-component receivers spread over 1000 m across the

Y.-G. Li and K. Aki, Department of Earth Sciences, University of Southern California, Los Angeles, CA 90089, USA.
J. E. Vidale and W. H. K. Lee, U.S. Geological Survey, Menlo Park, CA 94025, USA.
C. J. Marone, Department of Earth, Atmospheric, and Planetary Sciences, Massachusetts Institute of Technology, Cambridge, MA 02139, USA.
*To whom correspondence should be addressed.